How Do Ambient Conditions Influence Sorbent Selection in Adsorption-Based Direct Air Capture?[†]

Malte Glaser,[a] Arvind Rajendran,[b] and Sean T. McCoy*[a]

S Supplementary Information

S.1 DAC Model Development

Tables S1 and S2 list parameters used in the development of the 0-D model. They detail the dimensions of the modelled adsorption column, the heat and mass transfer within the adsorption column, and specific parameters related to the sorbents considered. For validation purposes and comparison, most parameters are sourced from Balasubramaniam *et al.* [1], with some adjustments made for the purposes of this study. Most importantly, even though some of these parameters may vary during the direct air capture (DAC) cycle, they are assumed to be constant regardless of the conditions in the adsorption column, primarily due to the lack of more accurate data. For instance, the vacuum pump efficiency is assumed to remain constant at 72 %. Although this value is likely too optimistic for low-pressure operation, it is maintained to ensure consistency with the 1-D model used for validation. However, since this assumption only affects the electrical energy demand—which is several times smaller than the thermal energy demand—the impact of vacuum pump efficiency on the overall results of this study is negligible. For more information on the influence of different parameters on the model's performance, refer to Balasubramaniam *et al.* [1], who conducted several sensitivity analyses on their model.

Table S1 Dimensions and parameters of the modelled adsorption column

Parameter	Description	Value	Unit
r_{in}	inner adsorption column radius [1]	0.040	m
r_{out}	outer adsorption column radius [1]	0.041	m
l	adsorption column length [1]	0.01	m
$y^{I}_{\mathrm{CO_2}}$	inlet CO_2 concentration [1]	400	ppm
$e_{\mathrm{energy,CO_2,eq}}$	on-site energy emissions [2]	0.184	$\mathrm{kg\,kW^{-1}\,h^{-1}}$
h_{in}	inner heat transfer coefficient [1]	3	$\mathrm{W\,m^{-2}\,K^{-1}}$
h_{out}	outer heat transfer coefficient [3]	26	$\mathrm{W\,m^{-2}\,K^{-1}}$
$c_{\mathrm{p,CO_2}}$	specific heat capacity, CO_2 [4]	36.04	$\mathrm{J\,mol^{-1}\,K^{-1}}$
$c_{\mathrm{p,H_2O,g}}$	specific heat capacity, H_2O, gas [1]	37.44	$\mathrm{J\,mol^{-1}\,K^{-1}}$
$c_{\mathrm{p,H_2O,l}}$	specific heat capacity, H_2O, liquid [1]	73.10	$\mathrm{J\,mol^{-1}\,K^{-1}}$
$c_{\mathrm{p,N_2}}$	specific heat capacity, N_2 [5]	29.09	$\mathrm{J\,mol^{-1}\,K^{-1}}$
$k_{\mathrm{CO_2}}$	mass transfer coefficient, CO_2 [1]	0.0002	$\mathrm{s^{-1}}$
$k_{\mathrm{H_2O}}$	mass transfer coefficient, H_2O [1]	0.2	$\mathrm{s^{-1}}$
ρ^{W}	wall density [1]	7800	$\mathrm{kg\,m^{-3}}$
c^{W}_{p}	specific heat capacity, wall [6]	0.502	$\mathrm{J\,g^{-1}\,K^{-1}}$
γ	adiabatic constant [1]	1.4	-
η_{Fan}	fan efficiency [1]	0.72	-
η_{VP}	vacuum pump efficiency [1]	0.72	-
$\Delta H_{\mathrm{vap,H_2O}}$	heat of vaporisation, H_2O [1]	42300	$\mathrm{J\,mol^{-1}}$
$\Delta H_{\mathrm{sub,H_2O}}$	heat of sublimation, H_2O, [7]	51040	$\mathrm{J\,mol^{-1}}$

A major difference between different DAC models published in the literature lies in the underlying isotherm models, which describe the relationship between sorbent loading, temperature, and relative humidity. Figure S1 illustrates the impact of relative humidity on sorbent loading for the sorbents considered, plotted on a logarithmic scale of CO_2 partial pressure, based on the isotherm model used in Balasubramaniam *et al.* [1]. Accordingly, the isotherm model used in this study also predicts negative loadings for SIFSIX-18-Ni-β (SIFSIX) and NbOFFIVE-1-Ni (NbOFFIVE) when relative humidity exceeds 90 % and 75 %, respectively. To address this, the model assumes zero loading beyond these thresholds, corresponding to the predicted values at 90 % (for SIFSIX) and 75 % relative humidity (for NbOFFIVE). This behaviour is illustrated in Figure S1, where the isotherms for both materials converge and remain at zero once the respective humidity thresholds are exceeded (see yellow lines in the middle and bottom subplots). The figure also demonstrates that raising relative humidity, particularly for APDES-NFC-FD-S (APDES), a chemisorbent, increases CO_2 equilibrium loading, whereas other sorbents show reduced CO_2 equilibrium loading. This explains the results of this study, emphasising the impact of humidity on DAC performance. While APDES often achieves the highest CO_2 loading, it also results in increased H_2O adsorption. Therefore, depending on the associated on-site energy emissions, the additional energy required for H_2O desorption may outweigh the benefits of increased CO_2 capture. Conversely, SIFSIX and NbOFFIVE show less H_2O adsorption, making it more beneficial, particularly under dry conditions, despite lower CO_2 capture capacities.

Figure S2 presents the results of the 0-D and 1-D models for the SIFSIX sorbent, using the same validation approach applied to APDES—namely, implementing the cycle designs from Balasubramaniam *et al.* [1] and comparing SED and Pr. The results from the calibrated 0-D and 1-D models show good agreement, supporting their use in evaluating DAC performance for the purposes of this study. This agreement is particularly strong in the range of low SED and low productivity, which is likely where DAC systems will operate, as high energy demand is probably undesirable. For NbOFFIVE, however, insufficient data is available

---

*[a] *Department of Chemical and Petroleum Engineering, University of Calgary, 2500 University Drive NW, Calgary, T2N 1N4, Alberta, Canada. E-mail: sean.mccoy@ucalgary.ca*

[b] *Department of Chemical and Materials Engineering, University of Alberta, 12th Floor, Donadeo Innovation Center for Engineering, 9211 116 St NW, Edmonton, AB T6G 1H9, Alberta, Canada. E-mail: arvind.rajendran@ualberta.ca*

Table S2 Sorbent-specific parameters[1]

(a) APDES

Parameter	Description	Value	Unit
$r_{\mathrm{p}}^{\mathrm{APDES}}$	particle radius	0.00375	m
$\varepsilon^{\mathrm{APDES}}$	bed voidage	0.092	-
ρ^{APDES}	density	61	$\mathrm{kg\,m^{-3}}$
$c_{\mathrm{p}}^{\mathrm{APDES}}$	specific heat capacity	2.07	$\mathrm{J\,g^{-1}\,K^{-1}}$
$\Delta H_{\mathrm{ads,CO_2}}^{\mathrm{APDES}}$	heat of adsorption	60000	$\mathrm{J\,mol^{-1}}$
$\Delta H_{\mathrm{ads,H_2O}}^{\mathrm{APDES}}$	heat of adsorption	43800	$\mathrm{J\,mol^{-1}}$

(b) SIFSIX

Parameter	Description	Value	Unit
$r_{\mathrm{p}}^{\mathrm{SIFSIX}}$	particle radius	0.00375	m
$\varepsilon^{\mathrm{SIFSIX}}$	bed voidage	0.4	-
ρ^{SIFSIX}	density	786	$\mathrm{kg\,m^{-3}}$
$c_{\mathrm{p}}^{\mathrm{SIFSIX}}$	specific heat capacity	1	$\mathrm{J\,g^{-1}\,K^{-1}}$
$\Delta H_{\mathrm{ads,CO_2}}^{\mathrm{SIFSIX}}$	heat of adsorption	52000	$\mathrm{J\,mol^{-1}}$
$\Delta H_{\mathrm{ads,H_2O}}^{\mathrm{SIFSIX}}$	heat of adsorption	45036	$\mathrm{J\,mol^{-1}}$

(c) NbOFFIVE

Parameter	Description	Value	Unit
$r_{\mathrm{p}}^{\mathrm{NbOFFIVE}}$	particle radius	0.00375	m
$\varepsilon^{\mathrm{NbOFFIVE}}$	bed voidage	0.4	-
ρ^{NbOFFIVE}	density	1173.6	$\mathrm{kg\,m^{-3}}$
$c_{\mathrm{p}}^{\mathrm{NbOFFIVE}}$	specific heat capacity	1	$\mathrm{J\,g^{-1}\,K^{-1}}$
$\Delta H_{\mathrm{ads,CO_2}}^{\mathrm{NbOFFIVE}}$	heat of adsorption	50000	$\mathrm{J\,mol^{-1}}$
$\Delta H_{\mathrm{ads,H_2O}}^{\mathrm{NbOFFIVE}}$	heat of adsorption	45036	$\mathrm{J\,mol^{-1}}$

to enable proper validation using the same methodology as for SIFSIX and APDES. Nonetheless, the results from individual cycle simulations yielded KPIs within a ± 10 % range.

S.2 Integration of Ambient Conditions

Figure S3 illustrates the error introduced through temporal aggregation in comparison to real-world ambient conditions. The analysis covered 1 to 10 typical periods (TP) and 1 to 10 days per typical period. For each number of typical periods, the legend depicts the optimal number of days per period that minimises the error for that number of TPs. With four typical periods and eight days per period, the error becomes sufficiently small. Beyond this point, additional typical periods do not considerably decrease the error further. Therefore, the analysis uses four typical periods of 8 days each, which could be interpreted as representing four typical seasons of a year.

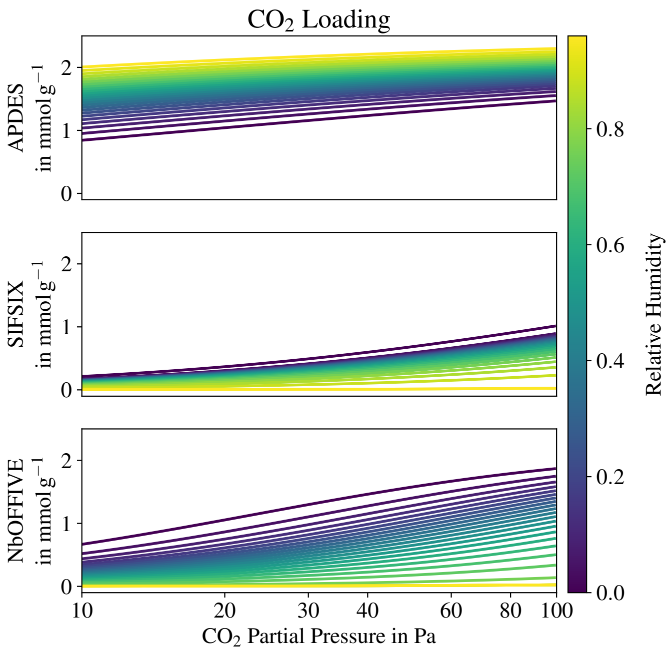

Fig. S1 Influence of varying relative humidity levels on $\mathrm{CO_2}$ isotherms for three different sorbents at $T = 20\ ^\circ\mathrm{C}$

S.3 Optimisation

Tables S3 and S4 present the defined constraints for decision variables and constant cycle design parameters. Particle swarm algorithm (PSA) is employed to optimise the DAC model using 10,000 particles, with the process terminating upon convergence. Since this study focuses on sorbent selection, convergence is defined as the point at which PSA prioritises a single sorbent, and CRR cannot be further improved by altering the sorbent. However, this does not imply that the optimal cycle design is found, as this aspect falls outside the scope of the current study. Figure S4 illustrates the optimisation progress for TP1 and TP2 in Calgary. The figure depicts the top 100 particles for each iteration, with the best particle indicated by a larger marker. After just nine iterations, the optimisation no longer improves the CRR by changing the sorbent type.

Table S3 Constraints for cycle design decision variables

Variable	Min Value	Max Value	Unit
τ_{ads}	1000	40000	s
τ_{des}	1000	40000	s
p_{des}	1000	40000	Pa
v_{ads}	1	150	$\mathrm{cm\,s^{-1}}$
v_{steam}	0.01	150	$\mathrm{cm\,s^{-1}}$

Table S4 Assumed constant cycle design parameters

Parameter	Value	Unit
τ_{eva}	100	s
τ_{ht}	400	s
T_{des}	120	°C

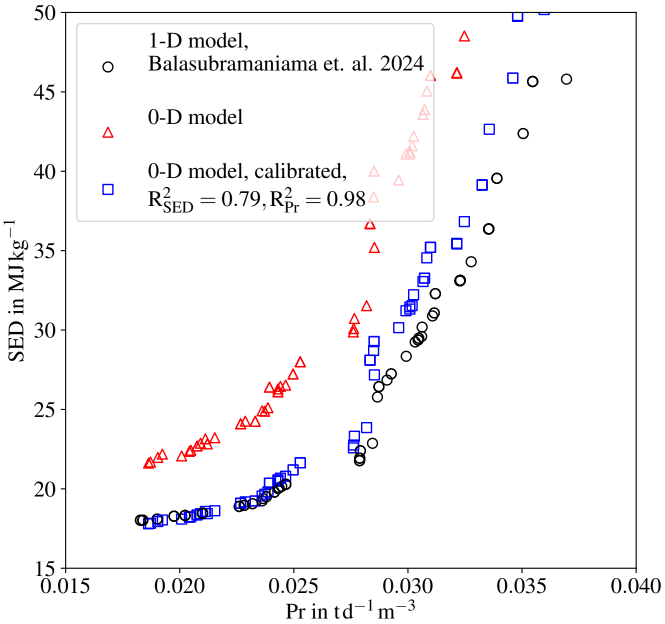

Fig. S2 Comparison of calculated specific energy demand (SED) and productivity (Pr) for various steam-assisted cycle designs using SIFSIX sorbent, between 1-D model, 0-D model, and calibrated 0-D model

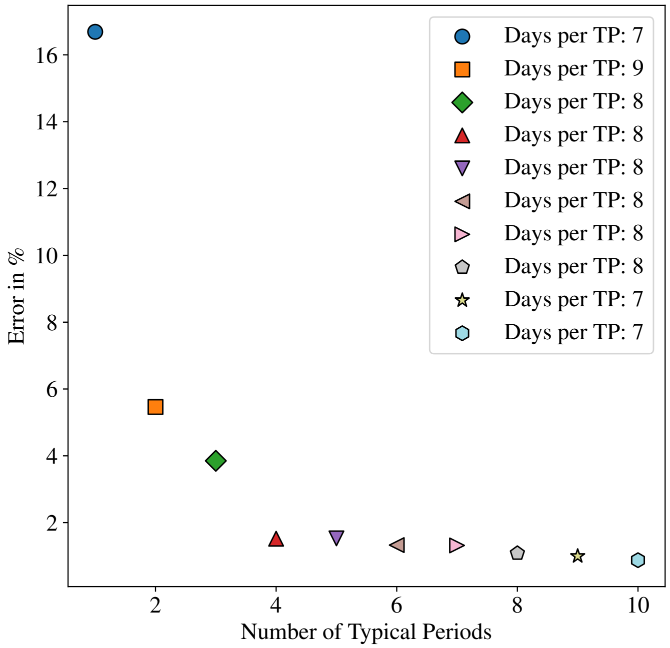

Fig. S3 Introduced error through temporal aggregation using a hierarchical aggregation algorithm, depending on the number of typical periods and days per typical period

S.4 Impact of k_{H_2O} on Model Performance

Figure S5 illustrates the influence of different values of k_{H_2O} on CO_2 and H_2O loading in the system for the three sorbents considered and the cycle design outlined in Table 3. The results show that varying k_{H_2O} from 0.2 to 0.0002 has only a marginal effect on CO_2 loading. Similarly, the impact on H_2O loading is minimal for $k_{H_2O} \in 0.2, 0.02, 0.002$, with noticeable differences observed only at $k_{H_2O} = 0.0002$. However, based on experimental data, the mass transfer of H_2O is expected to be much faster than that of CO_2 [8,9]. Thus, the results presented in Figure S5 suggest that the findings of this study hold across a wide range of k_{H_2O} values. This is further supported by the fact that the choice of sorbent in the case studies in Section 3 remains consistent when different mass transfer coefficients are applied.

This is because the rates of adsorption and desorption depend on both the mass transfer coefficient and the difference between the equilibrium and current loading, $\Delta q_i^A = (q_i^{A,*} - q_i^A)$. A higher mass transfer coefficient reduces Δq_i^A more quickly, allowing the column to reach equilibrium faster and reducing the adsorption/desorption rate. In contrast, a lower coefficient slows the initial rate of adsorption/desorption, but the larger Δq_i^A in subsequent iterations compensates, causing equilibrium to be reached one iteration later (see grey dotted line between each marker). This effect is shown in the bottom subplot of Figure S5, where the green crosses overcome Δq_i^A and catch up within one computational iteration. However, if k_{H_2O} is too small, the larger Δq_i^A cannot compensate for the slow mass transfer within the next computational step, as indicated by the black squares in the bottom subplot, which never reach the level of the blue or green markers. This phenomenon was observed for different computational step sizes, with only minor differences seen when the step size was reduced to less than a second. However, this would increase the computational load required to solve the system of ordinary differential equations.

S.5 Artificial Ambient Conditions

The use of artificial ambient conditions aims to analyse the impact of temperature, relative humidity, and their relative variations on sorbent selection. Depending on the level of variation, ambient conditions fluctuate around a base value of temperature and relative humidity as shown in Figure S6. Ambient conditions are allowed to fluctuate between two boundaries, specifically 250 K and 350 K for temperature, and 0 % and 95 % for relative humidity. Relative variations in this case consider the difference between the base value and the corresponding minimum or maximum value investigated (i.e., for a base value of 293 K and 60 % variation, the artificial ambient conditions are represented by a sine curve fluctuating between $293 + 0.6 \cdot (293 - 250) = 318.8$ K and $293 - 0.6 \cdot (293 - 250) = 267.2$ K). The model is then optimised for the entire range of artificial ambient conditions.

S.6 Impact of Ambient Conditions on Model Performance

Figure S7 compares the temporal variations in net carbon removal rate (CRR), H_2O loading, and CO_2 loading for the sorbents APDES and SIFSIX in Calgary, in response to varying ambient conditions accounted for by the model. The results indicate that the specific sorbent loading is higher for APDES than for SIFSIX. However, in absolute terms, SIFSIX captures a greater mass of CO_2 and H_2O than APDES, as shown by the comparisons of $\Delta m_{CO_2,\text{cycle}}$ and $\Delta m_{H_2O,\text{cycle}}$ in Tables S5a and S5b, respectively. The absolute increase in H_2O capture (297.65/273.53, corresponding to a 9 %

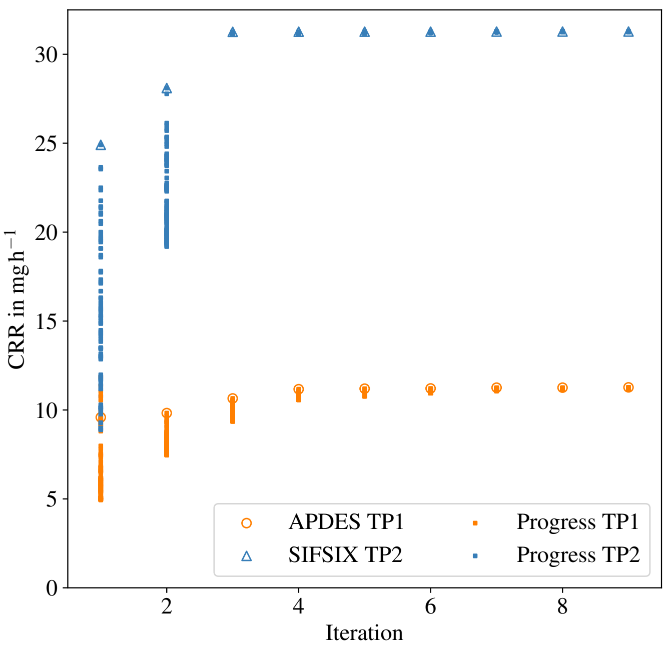

Fig. S4 Optimisation progress for Calgary for typical periods 1 and 2 (TP1, TP2), using 10,000 particles, with larger markers indicating the best particle in each iteration

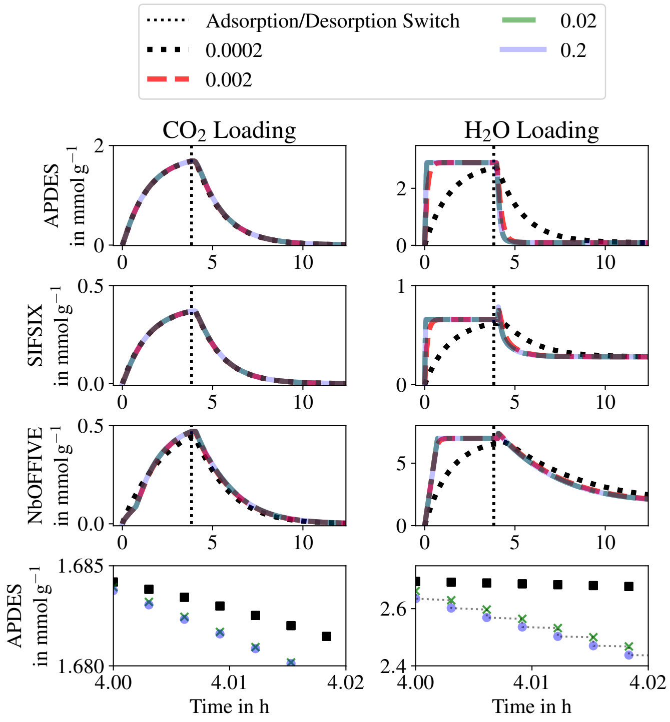

Fig. S5 Influence of different values of k_{H_2O} on CO_2 and H_2O loading for three different sorbents. The bottom plots provide a detailed snapshot of the desorption step, highlighting the marginal differences in model results arising from variations in the mass transfer coefficient.

increase in Cycle 1) is outweighed by a greater increase in CO_2 capture (491.04/214.72, corresponding to a 129 % increase in Cycle 1). This partly explains the higher CRR for the SIFSIX system, reinforcing the general preference for SIFSIX over APDES in Calgary.

Furthermore, during the first two cycles, ambient conditions remain relatively stable, resulting in minimal changes in key model variables and CRR, regardless of the sorbent used. However, in Cycles 3 and 4, ambient relative humidity and temperature decrease. For SIFSIX, this leads to a reduction in H_2O loading due to the lower availability of atmospheric moisture, decreasing by 22.5 % from Cycle 1 to Cycle 4 (0.62/0.8). As a result, adsorption sites previously occupied by H_2O molecules become available for CO_2 adsorption, leading to a 38 % increase in CO_2 loading over the same period (0.65/0.47), as shown in Figure S7a. This shift contributes to a 148 % increase in CRR (32.3/13) for the SIFSIX system in the same time frame. A similar but less pronounced effect is observed for APDES, with a 2 % decrease in CO_2 loading (1.72/1.75) and a 36 % decrease in H_2O loading (3.49/5.46). Despite the reduction in CO_2 loading, CRR for APDES still increases by 150 % (6.27/2.51), which can be attributed to a lower absolute energy demand (AED) during this time frame.

Figure S8 presents a similar analysis for Barbados. As previously discussed, Barbados is warmer and more humid than Calgary, resulting in a comparatively lower CO_2 loading (0.11/0.47, a 77 % decrease between Barbados and Calgary for the SIFSIX system in Cycle 1). This lower uptake contributes to a reduced CRR and, in the case of SIFSIX, even a negative CRR, indicating that its use would result in net positive rather than net negative emissions. In contrast, H_2O loading does not vary considerably between the two locations, as the assumed isotherms for H_2O adsorption are dependent solely on ambient relative humidity and not temperature[1]. Although Calgary has a much lower specific humidity than Barbados, both locations show similar relative humidity due to temperature differences, which explains the comparable H_2O loadings. While this assumption may not fully reflect real-world behaviour, it is adopted due to the lack of more reliable data on co-adsorption isotherms. Additionally, the figure indicates that the relatively stable ambient conditions in Barbados result in minimal variation in performance over time, as model results for both sorbents remain largely constant throughout the considered time frame.

As indicated above, the amount of CO_2 captured influences CRR; however, energy demand also plays a considerable role. To illustrate this, Figure S9 compares the key performance indicators (KPIs) for DAC performance per cycle for the sorbents APDES and SIFSIX in Calgary, using the same ambient conditions and cycle designs as in Figure S7. The figure shows that while the AED of the SIFSIX system is higher—partly due to the need to desorb greater amounts of H_2O and CO_2—its specific energy demand (SED) is lower than that of APDES. This is because SIFSIX captures more CO_2 overall, as indicated by the differences between the black dash-dotted lines in Figures S9a and S9b. Table S5 shows that in Cycle 1, although SIFSIX has a 95 % higher AED (7338.90/3763.25), this is offset by a 129 % increase in CO_2 capture (491.04/214.72), resulting in a 15 % reduction in SED (14.95/17.53). Likewise, while the higher AED increases on-site emissions, the greater CO_2 capture mitigates this effect, result-

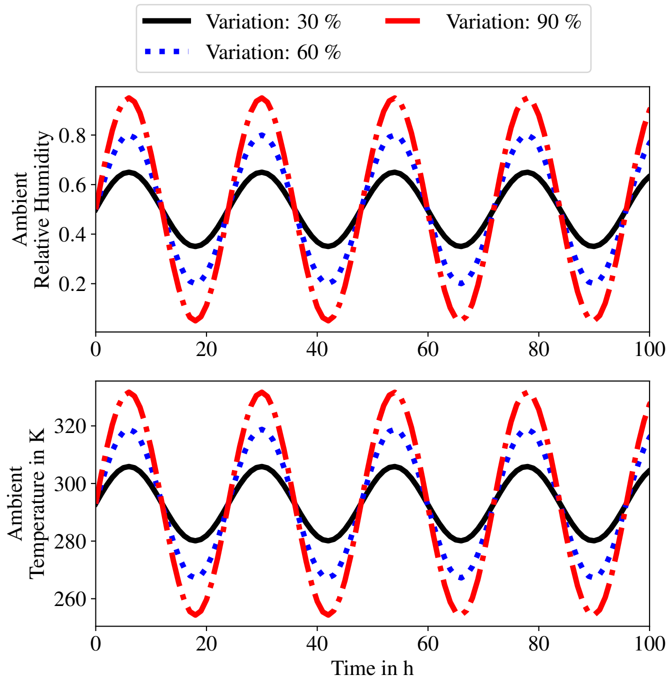

Fig. S6 Artificial ambient conditions based on base values $T_{\text{amb}} = 293$ K and $\varphi_{\text{amb}} = 50$ %, with different levels of variation

ing in a 418 % increase in CRR (13.00/2.51), as indicated by the purple lines in the figure.

Once again, the hourly variations in ambient conditions in Calgary influence the temporal trajectory of the model's KPIs. For the SIFSIX system, both CRR and the amount of CO_2 captured increase from Cycle 1 to Cycle 4. These trends are consistent with the increased CO_2 loading observed for SIFSIX in Figure S7a. However, as mentioned earlier, the rising CRR is driven not only by increased CO_2 capture but also by a lower SED. This is due to the decreasing relative humidity, which reduces H_2O loading and thus lowers the SED (11.27/14.95, a 25 % decrease from Cycle 1 to Cycle 4 for the SIFSIX system), as less energy is required to desorb excess water. For APDES, however, Figure S9a shows that the increase in CRR is solely due to the reduction in AED, as the total amount of CO_2 captured remains nearly constant (14.38/17.53, an 18 % decrease in SED, and 211.14/214.72, a 1.7 % decrease in CO_2 captured from Cycle 1 to Cycle 4).

Next to the effects different sorbents have under the same ambient conditions, comparing Figures S9 and S10 emphasises the variation in KPIs when DAC is deployed in different locations and under varying ambient conditions. The differences are particularly notable for the SIFSIX system between Calgary and Barbados, where, in Cycle 1, Barbados' AED is 38 % lower (4572.87/7338.90) than that of Calgary. However, the 77 % decrease in CO_2 capture (113.24/491.04) still leads to an overall increase in SED of 170 % (40.38/14.95) in Barbados compared to Calgary. This demonstrates that increasing the AED, and consequently on-site emissions, can be justified if it results in a higher CRR. The figure also shows that, similar to the model variables in Figure S8, the main KPIs do not change considerably over time in Barbados. Variations for the APDES system are minimal, while for the SIFSIX system, only SED varies notably over time, increasing by 13 % from Cycle 1 to Cycle 4 (45.67/40.38).

Figures S7 to S10 and Table S5 illustrate that describing DAC performance using a single fixed KPI value, such as a fixed benchmark energy demand, overlooks its actual variability and dynamics. More specifically, for the four cycles considered here, energy demand varies widely depending on the weather and sorbent used, ranging from as low as 11.27 $\mathrm{MJ\,kg^{-1}}$ to 45.67 $\mathrm{MJ\,kg^{-1}}$. Even more pronounced effects are expected over time and across locations with different ambient conditions.

Table S5 Detailed results for Calgary and Barbados

(a) Calgary, APDES

	Cycle 1	Cycle 2	Cycle 3	Cycle 4	Unit
$\Delta q_{CO_2,\text{cycle}}$	1.75	1.69	1.74	1.72	$\mathrm{mmol\,g^{-1}}$
$\Delta q_{H_2O,\text{cycle}}$	5.46	4.97	4.14	3.49	$\mathrm{mmol\,g^{-1}}$
SED	17.53	15.99	15.32	14.38	$\mathrm{MJ\,kg^{-1}}$
AED	3763.25	3316.07	3264.64	3036.72	J
$\Delta m_{CO_2,\text{cycle}}$	214.72	207.39	213.14	211.14	mg
$\Delta m_{H_2O,\text{cycle}}$	273.53	249.28	207.50	174.80	mg
$\Delta m_{CO_2,\text{on-site}}$	192.34	169.49	166.86	155.21	mg
CRR	2.51	4.25	5.19	6.27	$\mathrm{mg\,h^{-1}}$

(b) Calgary, SIFSIX

	Cycle 1	Cycle 2	Cycle 3	Cycle 4	Unit
$\Delta q_{CO_2,\text{cycle}}$	0.47	0.46	0.64	0.65	$\mathrm{mmol\,g^{-1}}$
$\Delta q_{H_2O,\text{cycle}}$	0.80	0.70	0.67	0.62	$\mathrm{mmol\,g^{-1}}$
SED	14.95	14.00	11.70	11.27	$\mathrm{MJ\,kg^{-1}}$
AED	7338.90	6787.04	7767.23	7661.58	J
$\Delta m_{CO_2,\text{cycle}}$	491.04	484.63	663.67	679.77	mg
$\Delta m_{H_2O,\text{cycle}}$	297.65	262.87	248.93	229.87	mg
$\Delta m_{CO_2,\text{on-site}}$	375.10	346.89	396.99	391.59	mg
CRR	13.00	15.44	29.89	32.30	$\mathrm{mg\,h^{-1}}$

(c) Barbados, APDES

	Cycle 1	Cycle 2	Cycle 3	Cycle 4	Unit
$\Delta q_{CO_2,\text{cycle}}$	1.39	1.35	1.41	1.41	$\mathrm{mmol\,g^{-1}}$
$\Delta q_{H_2O,\text{cycle}}$	2.73	3.11	3.03	3.21	$\mathrm{mmol\,g^{-1}}$
SED	16.83	16.58	17.26	17.61	$\mathrm{MJ\,kg^{-1}}$
AED	2863.42	2750.33	2980.40	3043.40	J
$\Delta m_{CO_2,\text{cycle}}$	170.11	165.89	172.72	172.78	mg
$\Delta m_{H_2O,\text{cycle}}$	137.10	156.06	152.14	160.79	mg
$\Delta m_{CO_2,\text{on-site}}$	146.35	140.57	152.33	155.55	mg
CRR	2.66	2.84	2.29	1.93	$\mathrm{mg\,h^{-1}}$

(d) Barbados, SIFSIX

	Cycle 1	Cycle 2	Cycle 3	Cycle 4	Unit
$\Delta q_{CO_2,\text{cycle}}$	0.11	0.10	0.10	0.10	$\mathrm{mmol\,g^{-1}}$
$\Delta q_{H_2O,\text{cycle}}$	0.41	0.44	0.42	0.43	$\mathrm{mmol\,g^{-1}}$
SED	40.38	42.22	43.25	45.67	$\mathrm{MJ\,kg^{-1}}$
AED	4572.87	4336.63	4610.75	4616.82	J
$\Delta m_{CO_2,\text{cycle}}$	113.24	102.71	106.62	101.10	mg
$\Delta m_{H_2O,\text{cycle}}$	154.19	163.03	158.04	159.53	mg
$\Delta m_{CO_2,\text{on-site}}$	233.72	221.65	235.66	235.97	mg
CRR	-13.51	-13.33	-14.47	-15.12	$\mathrm{mg\,h^{-1}}$

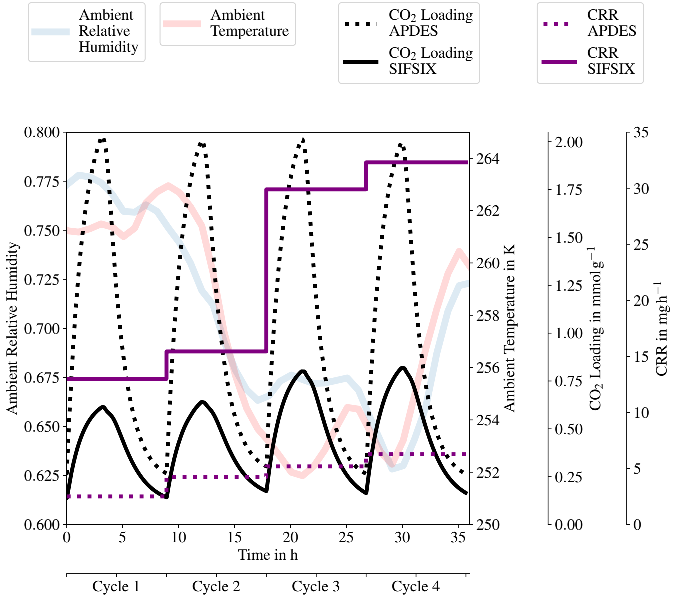

(a) CO_2 loading vs. ambient conditions and CRR in Calgary

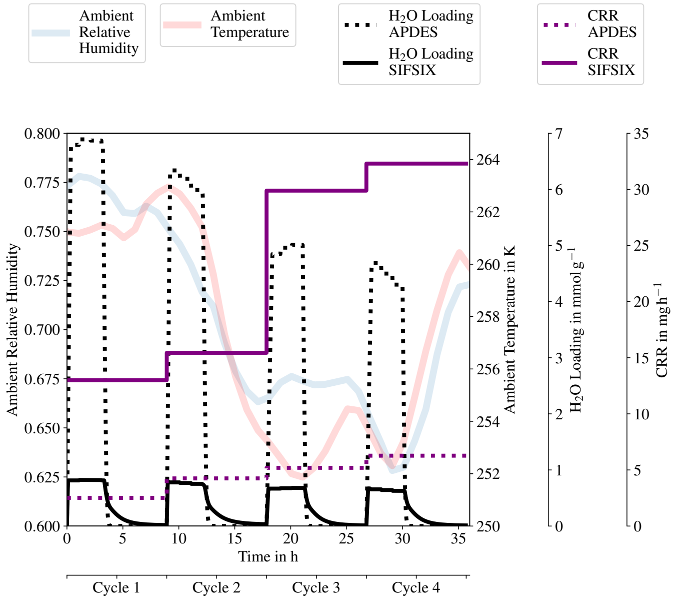

(b) H_2O loading vs. ambient conditions and CRR in Calgary

Fig. S7 Comparison of changes over time in ambient relative humidity, ambient temperature, CRR, H_2O loading, and CO_2 loading for the sorbents APDES and SIFSIX. Weather inputs are based on data from Calgary from January 1st 2023 at 08:00 to January 2nd 2023 at 20:00. The cycle design assumes an adsorption step duration of 3.13 h, desorption step duration of 5.65 h, air inlet velocity of 0.32 $\mathrm{m\,s^{-1}}$, and desorption pressure of 1162 Pa.

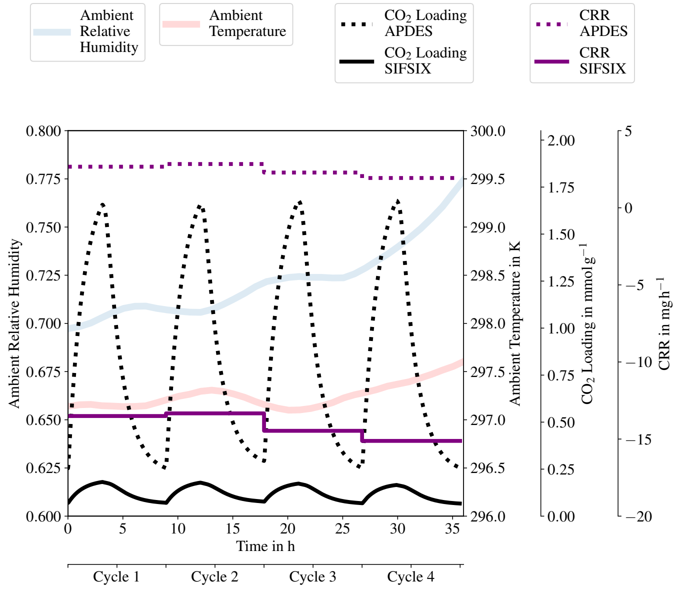

(a) CO_2 loading vs. ambient conditions and CRR in Barbados

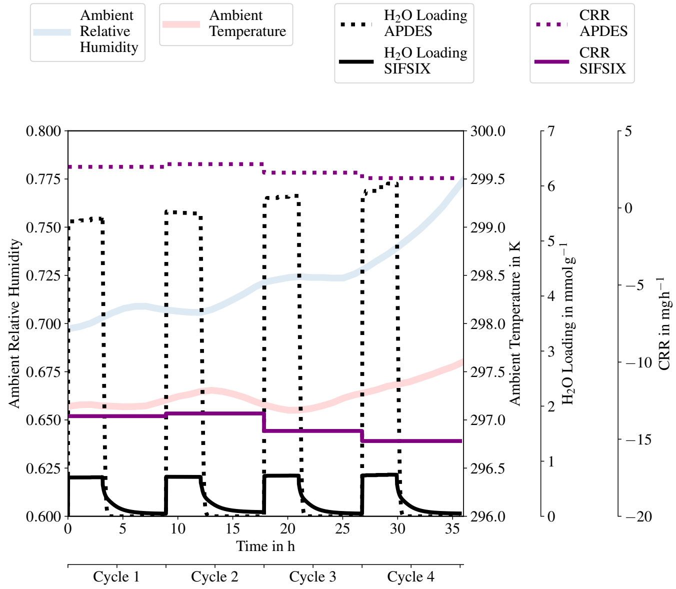

(b) H_2O loading vs. ambient conditions and CRR in Barbados

Fig. S8 Comparison of changes over time in ambient relative humidity, ambient temperature, CRR, H_2O loading, and CO_2 loading for the sorbents APDES and SIFSIX. Weather inputs are based on data from Barbados from January 1st 2023 at 08:00 to January 2nd 2023 at 20:00. The cycle design assumes an adsorption step duration of 3.13 h, desorption step duration of 5.65 h, air inlet velocity of 0.32 $\mathrm{m\,s^{-1}}$, and desorption pressure of 1162 Pa.

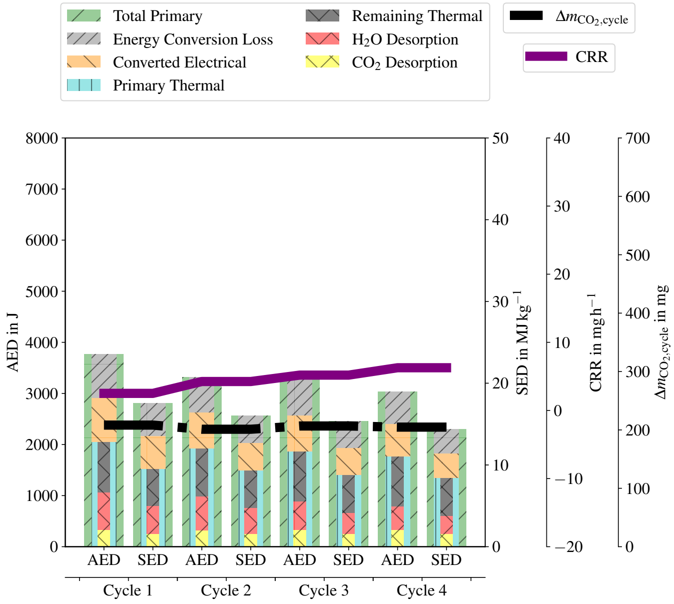

(a) Calgary, APDES

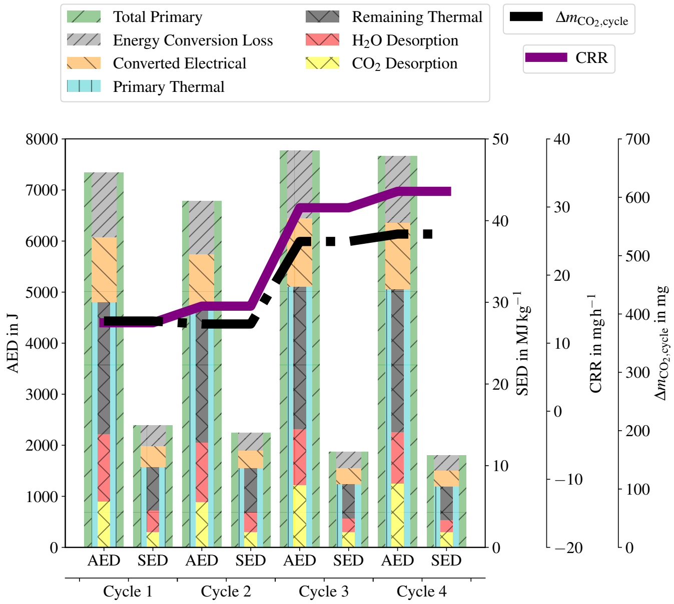

(b) Calgary, SIFSIX

Fig. S9 Comparison of DAC performance KPIs per cycle for the sorbents APDES and SIFSIX, covering both absolute and specific values. The total thermal energy demand consists of electrical energy demand, thermal energy demand (divided into CO_2 desorption, H_2O desorption, and other thermal components), and energy conversion losses. Additionally, CRR and the mass of CO_2 captured are reported. Weather inputs are based on data from Calgary from January 1st 2023 at 08:00 to January 2nd 2023 at 20:00. The cycle design assumes an adsorption step duration of 3.13 h, desorption step duration of 5.65 h, air inlet velocity of 0.32 $\mathrm{m\,s^{-1}}$, and desorption pressure of 1162 Pa.

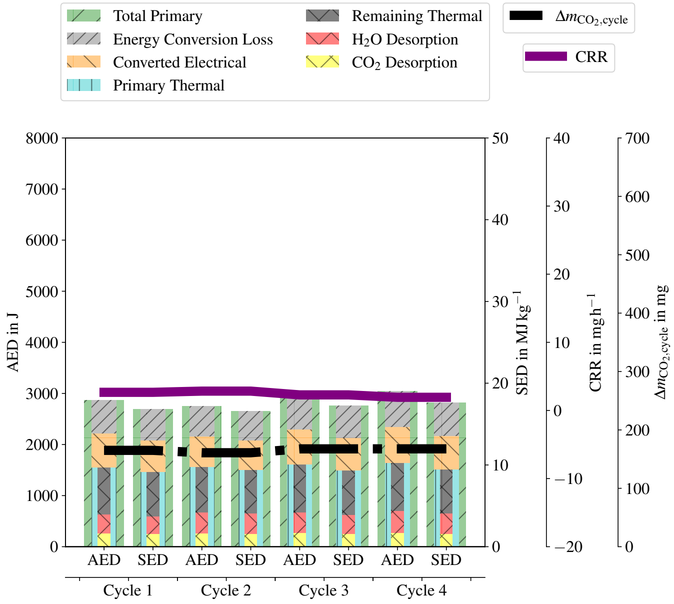

(a) Barbados, APDES

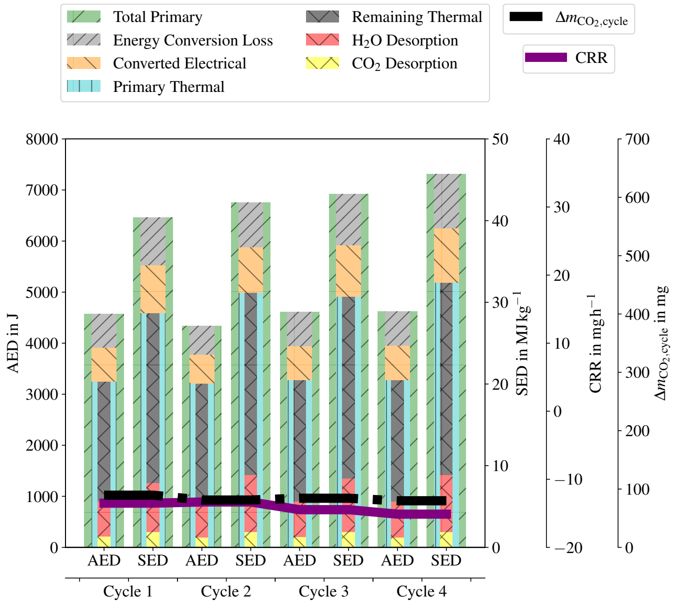

(b) Barbados, SIFSIX

Fig. S10 Comparison of DAC performance KPIs per cycle for the sorbents APDES and SIFSIX, covering both absolute and specific values. The total thermal energy demand consists of electrical energy demand, thermal energy demand (divided into CO_2 desorption, H_2O desorption, and other thermal components), and energy conversion losses. Additionally, CRR and the mass of CO_2 captured are reported. Weather inputs are based on data from Barbados from January 1st 2023 at 08:00 to January 2nd 2023 at 20:00. The cycle design assumes an adsorption step duration of 3.13 h, desorption step duration of 5.65 h, air inlet velocity of 0.32 $\mathrm{m\,s^{-1}}$, and desorption pressure of 1162 Pa.

Notes and references

1 B. M. Balasubramaniam, P.-T. Thierry, S. Lethier, V. Pugnet, P. Llewellyn and A. Rajendran, *Chemical Engineering Journal*, 2024, **485**, 149568.

2 SEAI, *Conversion and emission factors for publication*, 2023, `https://www.seai.ie/data-and-insights/seai-statistics/conversion-factors/`.

3 V. Stampi-Bombelli, M. Van Der Spek and M. Mazzotti, *Adsorption*, 2020, **26**, 1183–1197.

4 T. E. ToolBox, *Carbon Dioxide - Specific Heat of Gas vs. Temperature*, 2005, `https://www.engineeringtoolbox.com/carbon-dioxide-d_974.html`.

5 T. E. ToolBox, *Nitrogen Gas - Specific Heat vs. Temperature*, 2005, `https://www.engineeringtoolbox.com/nitrogen-d_977.html`.

6 R. Haghpanah, A. Majumder, R. Nilam, A. Rajendran, S. Farooq, I. A. Karimi and M. Amanullah, *Ind. Eng. Chem. Res.*, 2013, **52**, 4249–4265.

7 C. E. Bryson, V. Cazcarra and L. L. Levenson, *J. Chem. Eng. Data*, 1974, **19**, 107–110.

8 J. A. Wurzbacher, C. Gebald, N. Piatkowski and A. Steinfeld, *Environ. Sci. Technol.*, 2012, **46**, 9191–9198.

9 C. J. E. Bajamundi, J. Koponen, V. Ruuskanen, J. Elfving, A. Kosonen, J. Kauppinen and J. Ahola, *Journal of CO2 Utilization*, 2019, **30**, 232–239.